2020

Consumptive coagulopathy of severe yellow fever occurs independently of hepatocellular tropism and massive hepatic injury

Adam L. Bailey

Liang-I Kang

Luiz Gonzaga Francisco de Assis Barros D'Elia Zanella

Cássia G. T. Silveira

Yeh-Li Ho

See next page for additional authors

Authors

Adam L. Bailey, Liang-I Kang, Luiz Gonzaga Francisco de Assis Barros D'Elia Zanella, Cássia G. T. Silveira, Yeh-Li Ho, Lander Foquet, Greg Bial, Broc T. McCune, Amaro Nunes Duarte-Neto, Archana Thomas, Hans-Peter Raué, Kathleen Byrnes, Esper G. Kallas, Mark K. Slifka, and Michael S. Diamond

Consumptive coagulopathy of severe yellow fever occurs independently of hepatocellular tropism and massive hepatic injury

Adam L. Bailey[a,1], Liang-I Kang[a], Luiz Gonzaga Francisco de Assis Barros D'Elia Zanella[b,c], Cássia G. T. Silveira[b], Yeh-Li Ho[d], Lander Foquet[e], Greg Bial[e], Broc T. McCune[f], Amaro Nunes Duarte-Neto[g], Archana Thomas[h], Hans-Peter Raué[h], Kathleen Byrnes[a], Esper G. Kallas[d], Mark K. Slifka[h], and Michael S. Diamond[a,f,i,j,1]

[a]Department of Pathology and Immunology, Washington University School of Medicine, St. Louis, MO 63110; [b]Division of Clinical Immunology and Allergy, School of Medicine, University of São Paulo, Sao Paulo, Brazil 01246 903; [c]State Civil Servant's Hospital, São Paulo, Brazil 04028-000; [d]Department of Infectious and Parasitic Diseases, School of Medicine, University of São Paulo, Sao Paulo, Brazil 01246 903; [e]Yecuris Corporation, Tualatin, OR 97062; [f]Department of Medicine, Washington University School of Medicine, St. Louis, MO 63110; [g]Department of Pathology, Clinical Hospital, School of Medicine, University of São Paulo, Sao Paulo, Brazil 01246 903; [h]Division of Neuroscience, Oregon National Primate Research Center, Oregon Health & Science University, Beaverton, OR 97006; [i]Department of Molecular Microbiology, Washington University School of Medicine, St. Louis, MO 63110; and [j]The Andrew M. and Jane M. Bursky Center for Human Immunology and Immunotherapy Programs, Washington University School of Medicine, St. Louis, MO 63110

Edited by Peter Sarnow, Stanford University School of Medicine, Stanford, CA, and approved November 2, 2020 (received for review July 6, 2020)

Yellow fever (YF) is a mosquito-transmitted viral disease that causes tens of thousands of deaths each year despite the long-standing deployment of an effective vaccine. In its most severe form, YF manifests as a hemorrhagic fever that causes severe damage to visceral organs. Although coagulopathy is a defining feature of severe YF in humans, the mechanism by which it develops remains uncertain. Hepatocytes are a major target of yellow fever virus (YFV) infection, and the coagulopathy in severe YF has long been attributed to massive hepatocyte infection and destruction that results in a defect in clotting factor synthesis. However, when we analyzed blood from Brazilian patients with severe YF, we found high concentrations of plasma D-dimer, a fibrin split product, suggestive of a concurrent consumptive process. To define the relationship between coagulopathy and hepatocellular tropism, we compared infection and disease in *Fah*$^{-/-}$, *Rag2*$^{-/-}$, and *Il2rγ*$^{-/-}$ mice engrafted with human hepatocytes (hFRG mice) and rhesus macaques using a highly pathogenic African YFV strain. YFV infection of macaques and hFRG mice caused substantial hepatocyte infection, liver damage, and coagulopathy as defined by virological, clinical, and pathological criteria. However, only macaques developed a consumptive coagulopathy whereas YFV-infected hFRG mice did not. Thus, infection of cell types other than hepatocytes likely contributes to the consumptive coagulopathy associated with severe YF in primates and humans. These findings expand our understanding of viral hemorrhagic disease and associated coagulopathy and suggest directions for clinical management of severe YF cases.

yellow fever virus | coagulopathy | pathogenesis | D-dimer | hepatitis

Yellow fever (YF) is caused by the yellow fever virus (YFV), an enveloped positive-sense RNA virus (family: Flaviviridae; genus: *Flavivirus*) that is transmitted by mosquitoes (1). Prior to the 20th century, YF was an epidemic disease that caused substantial morbidity and mortality throughout Africa and the Americas. While mosquito control measures and vaccination campaigns have curbed the spread of YFV in urban centers, a sylvatic reservoir is maintained in mosquitoes and nonhuman primates (NHP) in the tropical rainforests of Africa and South America (2–4). Activities that bring humans into contact with infected mosquitoes can result in zoonotic transmission of YFV, initiating outbreaks that are sustained in more densely populated areas by the anthropophilic *Aedes aegypti* mosquito. Recently, outbreaks of YF have occurred in Angola (2016) (5), the Democratic Republic of Congo (2016), Brazil (2016 to 2019) (6, 7), and Nigeria (2018 to 2019) (8). The World Health Organization (WHO) estimates an incidence of 200,000 YF cases per year, leading to ~30,000 to 60,000 deaths with the majority occurring in sub-Saharan Africa (9). Overall, 47 countries in Africa and the Americas are within the modern YFV-endemic zone, with 600 to 700 million people at risk for infection and an additional 400 million requiring vaccination to achieve the 80% herd immunity threshold that prevents urban YFV transmission (9–11). Although the YFV-17D live-attenuated vaccine is highly effective, production issues have resulted in global shortages (11–13). The expansion of *Aedes* mosquitos into Asia, Oceania, Central America, and North America has also raised concerns that YFV could spread into regions with large numbers of unvaccinated individuals and ecosystems that could support new sylvatic reservoirs (3, 14).

YF begins as a nonspecific febrile illness, from which the majority of infected individuals recover. However, ~30% of cases progress to a more severe form of the disease characterized by

Significance

Fatal cases of yellow fever are preceded by the development of hemorrhagic complications. While yellow fever virus is known to infect hepatocytes, the relationship between hepatocyte infection and the development of hemorrhage is currently undefined. Here, we identified high concentrations of D-dimer in the blood of yellow fever patients, indicative of a process that involves the activation and consumption of clotting factors. We then developed a mouse model in which only transplanted human hepatocytes could be infected at high levels. By examining clotting parameters in this model, we determined that hepatocyte infection alone is insufficient to cause the activation and consumption of coagulation factors observed in severe cases of yellow fever in humans and nonhuman primates.

Author contributions: A.L.B., E.G.K., and M.S.D. designed research; A.L.B., B.T.M., A.T., and H.-P.R. performed research; L.G.F.d.A.B.D.Z., C.G.T.S., Y.-L.H., L.F., G.B., A.N.D.-N., A.T., H.-P.R., E.G.K., and M.K.S. contributed new reagents/analytic tools; A.L.B., L.-I.K., K.B., E.G.K., M.K.S., and M.S.D. analyzed data; and A.L.B. and M.S.D. wrote the paper.

Competing interest statement: M.S.D. is a consultant for Inbios, Eli Lilly, Vir Biotechnology, NGM Biopharmaceuticals, and is on the Scientific Advisory Board of Moderna and Immunome. The Diamond laboratory has received funding unrelated to this project under sponsored research agreements from Moderna, Vir Biotechnology, and Emergent BioSolutions.

This article is a PNAS Direct Submission.

[1]To whom correspondence may be addressed. Email: adam.bailey@wustl.edu or diamond@wusm.wustl.edu.

First published December 2, 2020.

multiorgan failure, coagulopathy, hemorrhage, and shock. Approximately 50% of these severe cases are fatal (15, 16). Based on pathological studies, it has been presumed that the infection and injury of hepatocytes is central to the development of coagulation abnormalities and the resulting hemorrhage in YF. Hepatocytes are the principal producer of most circulating coagulation factors, and a decrease in factor production occurs after massive hepatocyte injury (2, 15, 16). However, YFV has a broad cellular tropism, and recent evidence suggests that extrahepatic targets of infection may contribute to the pathogenesis of severe YF (17–21). Indeed, it has been speculated that decreased clotting factor production alone cannot explain the extent of coagulopathy observed in severe YF and that a consumptive coagulopathy (which is a major component of the clinical disease process known as disseminated intravascular coagulopathy [DIC]) occurs as part of YF pathogenesis (15, 22). Consumptive coagulopathy contributes to the pathogenesis of other viral hemorrhagic fevers including Ebola virus (EBOV), as evidenced by a direct correlation between EBOV mortality and the primary laboratory measure of clotting factor consumption, plasma D-dimer concentration (23). Although treatment of YF patients with plasma exchange, which restores coagulation system function, has been used as an intervention to reduce the case fatality rate of YF (24), our understanding of how coagulopathy develops in severe YF remains limited (15, 17, 18, 22).

Given that various hepatic disease processes can tip the balance of the coagulation system into hypo- or hyper-coagulable states (both of which can manifest as hemorrhage) (25), we first set out to identify the type of coagulopathy that predominates in severe YF. To do this, we quantified plasma concentrations of D-dimer—a fibrin split product generated only in hypercoagulable (i.e., consumptive) states—in hospitalized patients with laboratory-confirmed YFV infection and in experimentally infected rhesus macaques. In these hosts, we found high concentrations of D-dimer, indicative of a consumptive coagulopathy. Next, we investigated the relationship between hepatocyte infection and coagulopathy in YF. For this, we developed a unique YFV infection model in fumarylacetoacetate hydrolase *[Fah]*$^{-/-}$, *Rag2*$^{-/-}$, and *Il2rγ*$^{-/-}$ (FRG) chimeric mice. Wild-type (WT) mice are naturally resistant to hepatic YFV infection via peripheral routes of inoculation and do not develop YF-induced hepatic disease or coagulopathy (26–30). However, FRG mice have three genetic lesions (*Fah*$^{-/-}$, *Rag2*$^{-/-}$, and *Il2rγ*$^{-/-}$ on a C57BL/6J background), which, together with specifically timed dietary modifications, facilitate the durable replacement of murine hepatocytes with transplanted human hepatocytes (31). FRG mice engrafted with human hepatocytes (hFRG) have two theoretical advantages for study of YFV pathogenesis and coagulopathy: human-origin hepatocytes that are susceptible to YFV infection and a humanized clotting cascade that can develop consumptive coagulopathy. Infected mice with human hepatocytes (hFRG) developed disease that recapitulated many features of YF in humans including massive hepatic infection and injury. However, YFV-infected hFRG mice did not develop a consumptive coagulopathy, suggesting that infection of hepatocytes is not the sole determinant of coagulopathy and hemorrhage in severe YF in humans.

Results

Coagulopathy in Human YF Is Consumptive. We quantified plasma D-dimer concentrations in patients with laboratory-confirmed YFV infection who were hospitalized in São Paulo, Brazil, during the 2018 to 2019 epidemic. Although previous analysis of this cohort (32) had demonstrated coagulopathy using a prothrombin time (PT) assay, the blood concentration of D-dimers, and thus the mechanism of coagulopathy, were not evaluated. We found that 29 of 33 (88%) patients had markedly elevated D-dimer concentrations during their hospitalization, with 13 of 33 (39%) having levels above the upper limit of assay quantification (10,000 ng/mL, or 200-fold greater than the upper limit of the reference range).

YFV Infects Human Hepatocytes in hFRG Mice. To define the relationship between coagulopathy and YFV hepatocellular tropism, we compared infection of hFRG mice to age- and diet-matched WT C57BL/6J mice, FRG mice engrafted with syngeneic mouse hepatocytes (muFRG), and rhesus macaques (*Macacca mulatta*), the gold-standard animal model of viscerotropic/hemorrhagic YF disease (15, 20, 22, 33, 34). Mice were inoculated intravenously (i.v.) with 2×10^5 focus-forming units (FFU) with a highly pathogenic West African strain of YFV, YFV-Dakar. This route and dose were chosen to simulate the viremia that occurs after the initial round of YFV replication at or near the site of natural inoculation (i.e., the skin), thus bypassing the peripheral replication sites that are resistant to YFV infection in the mouse. Macaques were inoculated via subcutaneous (s.c.) injection with 550 FFU (5×10^4 $TCID_{50}$) of YFV-Dakar. Upon inoculation with YFV-Dakar, adult WT C57BL/6 mice exhibited a variable disease course, with 6 of 10 mice exhibiting weight loss and succumbing to disease by 14 d post inoculation (dpi) (Fig. 1*A*). Weight loss trends of YFV-infected muFRG mice were comparable to those of YFV-infected WT mice, with 10 to 20% decreases in body mass apparent by 8 dpi. In contrast, hFRG mice lost weight more rapidly following inoculation, exhibiting 10 to 25% weight loss within 4 to 5 d of infection. Three of four macaques infected with YFV reached predetermined humane end points and required euthanasia by 6 dpi, but weight loss was not a defining characteristic of YF disease. Of note, one macaque did not display overt signs of disease, consistent with the ∼75% lethality rate observed in this model, as described previously (33).

To determine the viral tropism in these models, we measured infection levels in key target tissues when the animals became moribund or required euthanasia. For a direct comparison to hFRG mice which became moribund within 4 to 5 d of virus inoculation, we also evaluated tissue viral burden in muFRG mice at this time. Greater than 1×10^6 YFV genome copies were present in the plasma of infected macaques and hFRG mice at these time points, whereas substantially lower levels were detected in WT and muFRG mice (Fig. 1*B*). We observed a hepatotropic pattern of YFV infection in macaques and hFRG mice. In contrast, WT and muFRG mice had high levels of infection in the brain (Fig. 1 *C* and *D*) but not in the liver, as observed previously (19, 35–37).

We next evaluated liver pathology in YFV-infected hosts. Livers from YFV-infected hFRG mice exhibited a pale appearance upon gross examination, with areas of apparent hemorrhage. Histopathological analysis of livers from humans, macaques, and hFRG mice revealed features typical of YF (15), characterized by apoptotic and steatotic hepatocytes, areas of necrosis, and minimal inflammatory tissue reaction (Figs. 1*E* and 2). The percentage of liver tissue affected correlated with the plasma and liver viral burden in YFV-infected hFRG mice (Fig. 1*F*). Features characteristic of YFV infection in humans and macaques were isolated to distinct patches throughout the livers of YFV-infected hFRG mice and were completely absent in livers from YFV-infected wild-type or muFRG mice (Fig. 2). Patches of diseased tissue in hFRG mice localized to zones of engrafted human hepatocytes, which could be distinguished from murine hepatocytes by their smaller cell size, higher nuclear-to-cytoplasmic ratio, more uniform nuclear size, paler cytoplasm, and fumarylacetoacetate hydrolase (FAH) staining by immunohistochemistry (38) (Figs. 2 and 3). Areas that stained positively for FAH displayed substantial overlap with areas that stained positively for YFV RNA by in situ hybridization (Fig. 3*A*), and the disease features observed in hematoxylin and eosin-stained tissue sections were most prominent in areas with abundant YFV RNA (Fig. 3*B*).

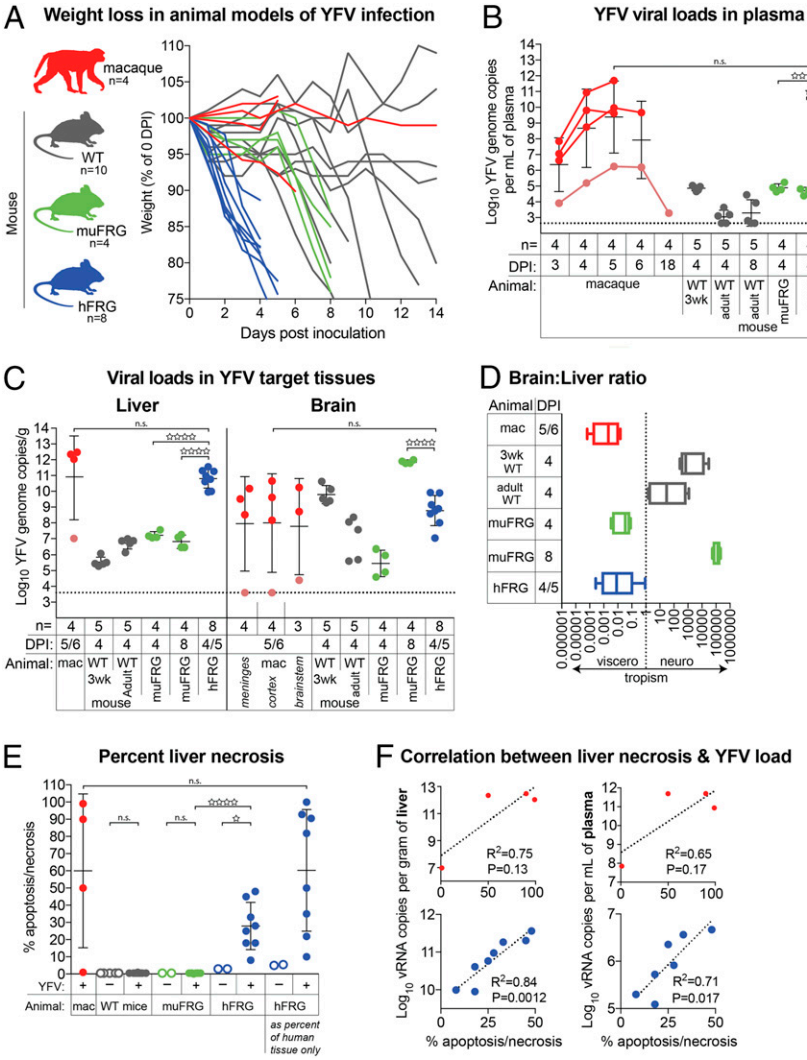

Fig. 1. YFV is viscerotropic in hFRG mice and macaques. (*A*) Weight-loss curves for macaques (mac), wild-type (WT) C57BL/6J mice (gray), muFRG mice (green), and hFRG mice (blue) following YFV inoculation. One macaque did not develop overt disease (denoted in salmon); this macaque was necropsied at day 18 post infection. (*B*) YFV viral load in plasma and (*C*) tissue homogenates, as determined by RT-qPCR. (*D*) Ratio of viral RNA load in brain versus liver, expressed as a ratio of the non–log-transformed value in each individual. (*E*) Quantification of apoptosis/necrosis in livers from YFV-infected macaques (red), muFRG mice (green), and hFRG mice (blue). Scoring of apoptosis/necrosis (and engraftment for hFRG mice, far right) was performed on hematoxylin- and eosin-stained sections by two board-certified hepatopathologists blinded to YFV-infection status. Data are the average of the two scores. (*F*) Linear regression of YFV burden in liver and plasma versus the percentage of liver scored as apoptosis/necrotic by examination of hematoxylin- and eosin-stained sections for YFV-infected macaques (red) and hFRG mice (blue). Statistical significance was determined from unpaired t tests performed on log-transformed values and is denoted by an open star (n.s.: $P \geq 0.05$; ☆: $P = 0.01$ to 0.05; ☆☆☆☆: $P < 0.0001$). The number of animals (n) for each experiment is indicated in *B* and *C*.

YFV Infection of hFRG Mice Recapitulates Key Features of Infection of Humans and Macaques. To correlate the disease observed in YFV-infected hFRG mice to humans, we compared key laboratory markers associated with end-organ damage. Markers of liver disease (e.g., alanine aminotransferase [ALT], total bilirubin, and ammonia [NH_3]) increased over the course of YFV infection in macaques and hFRG mice, but not in muFRG mice (Fig. 4 *A*, *C*, and *D*). By day 4/5, hFRG mice had reduced levels of albumin, indicative of a developing synthetic protein defect in the liver (Fig. 4*B*). Serum creatinine, a marker of renal function, was elevated in YFV-infected humans and macaques, but not in YFV-infected muFRG or hFRG mice (Fig. 4*E*). Finally, although pancreatitis was recently reported in some humans with severe YF (39), we found no significant increase in blood lipase in our animal models (Fig. 4*F*).

YFV Infection of hFRG Mice Fails to Induce Consumptive Coagulopathy. We assessed changes in coagulation over the course of YFV infection first by measuring prothrombin time (PT), a functional assay that evaluates clot formation via the extrinsic pathway (Fig. 5*A*). Prolongation of the PT beyond the reference range occurred in most YFV-infected macaques and in all hFRG mice, but not in any muFRG mice (Fig. 5*B*). Using factor-deficient plasmas, we performed mixing studies to analyze the activity of factors at various steps within the clotting cascade (Fig. 5*A*). We observed decreases in coagulation factor activities in macaques and muFRG and hFRG mice, as measured by activities of factor VII (extrinsic pathway), factor IX (intrinsic pathway), and factors II and X (common pathway) (Fig. 5*C*). However, the largest decreases occurred in hFRG mice. We did not detect consistent changes in factor VIII activity (intrinsic pathway) or fibrinogen levels (common pathway), both of which also are acute-phase reactants.

Unlike the functional PT assay, methods for quantifying blood D-dimer concentrations are antibody-based. Anti–D-dimer antibodies

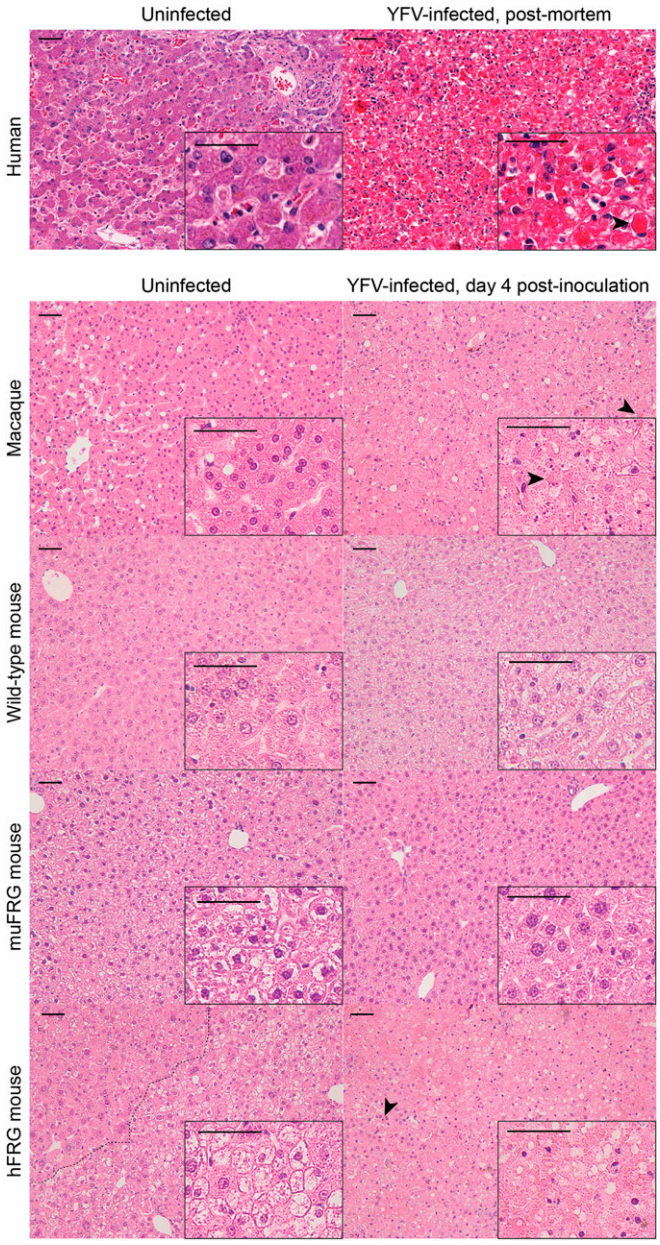

Fig. 2. Liver pathology in YFV-infected hFRG mice is similar to YFV-infected humans and macaques. Hematoxylin and eosin staining of FFPE liver sections collected from moribund naive and YFV-infected humans, macaques, wild-type mice, muFRG mice, and hFRG mice. Liver parenchyma is noticeably affected in humans, macaques, and hFRG mice, but not in wild-type or muFRG mice. Apoptotic cells, necrotic debris, and hypereosinophilic Councilman-Rocha-Lima bodies (arrowheads) are seen throughout the livers of affected hosts (Scale bars, 50 μm.)

generally recognize species-specific epitopes, complicating comparison of D-dimer concentrations across species or in animals with chimeric coagulation cascades. To examine the ability of various D-dimer assays to detect human, macaque, and murine D-dimers, we developed a method to generate D-dimers ex vivo using purified human plasmin. Plasmin lyses fibrin clots, liberating D-dimers in the process. We treated citrated plasma from uninfected macaques and hFRG mice with plasmin and demonstrated our ability to detect D-dimers in each of these species (Fig. 5*D*). After YFV infection, the three lethally infected macaques developed abnormally elevated blood concentrations of D-dimer within 4 to 5 d of infection (Fig. 5*E*). In contrast, we observed no significant elevations in D-dimer concentration in YFV-infected muFRG or hFRG mice (note: both human and murine D-dimer isoforms were measured in hFRG animals (Fig. 5*E*). Collectively, these data suggest that coagulopathy during YFV infection is host-dependent. In YFV-infected humans and macaques, coagulopathy is associated with both a synthetic defect and clotting factor consumption, whereas in hFRG mice only a synthetic defect is observed.

Discussion

The natural resistance of mice to YFV infection and disease has hampered pathogenesis studies and the development of therapeutics. To some degree, this obstacle is overcome by intracranial or i.v. inoculation of YFV, although the resulting encephalitis has questionable relevance to the viscerotropic disease observed in humans (40, 41). Some transgenic mice, particularly those lacking genes involved in type I IFN signaling, have enhanced susceptibility to YFV infection (17, 19, 26, 27, 28), although these animals still fail to develop the severe liver damage and coagulopathy that defines YF in humans (19, 28). With the possible exception of the Syrian hamster, which develops elevated ALT and prolonged PT but has not had D-dimer levels assessed (42, 43), NHPs remain the only laboratory animals that recapitulate these key aspects of human YF disease.

We developed a unique YFV infection model in FRG mice. Comparison of FRG mice engrafted with human (hFRG) or murine (muFRG) hepatocytes demonstrated the susceptibility of

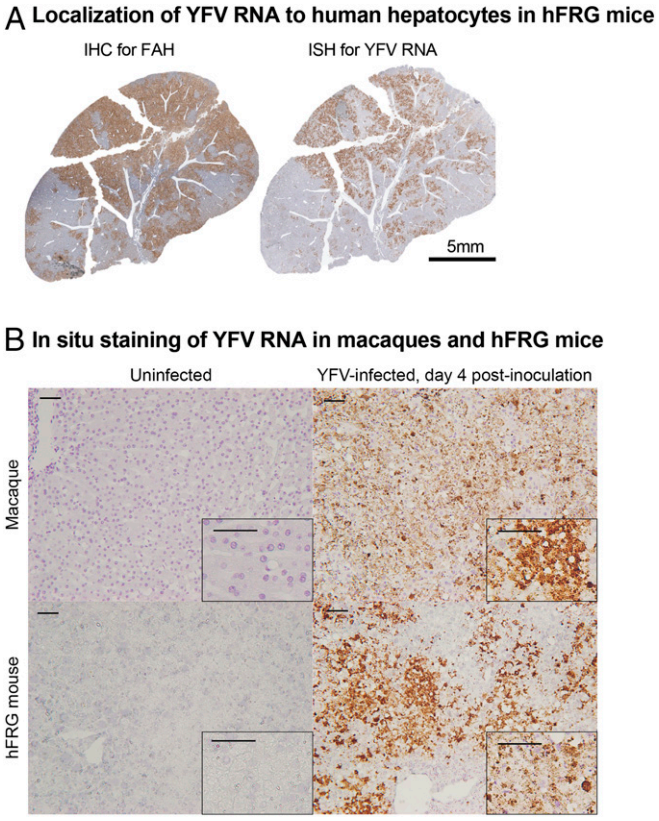

Fig. 3. YFV infects and destroys human and macaque hepatocytes, but not murine hepatocytes. (*A*) Low-magnification photographs of serial FFPE liver sections from a moribund hFRG mouse stained brown for FAH using IHC (*Left*) and YFV RNA using in situ hybridization (ISH) (*Right*). (*B*) ISH for YFV RNA in areas of prominent tissue damage in macaques and murine livers, counterstained with hematoxylin (Scale bars, 50 μm.)

MICROBIOLOGY

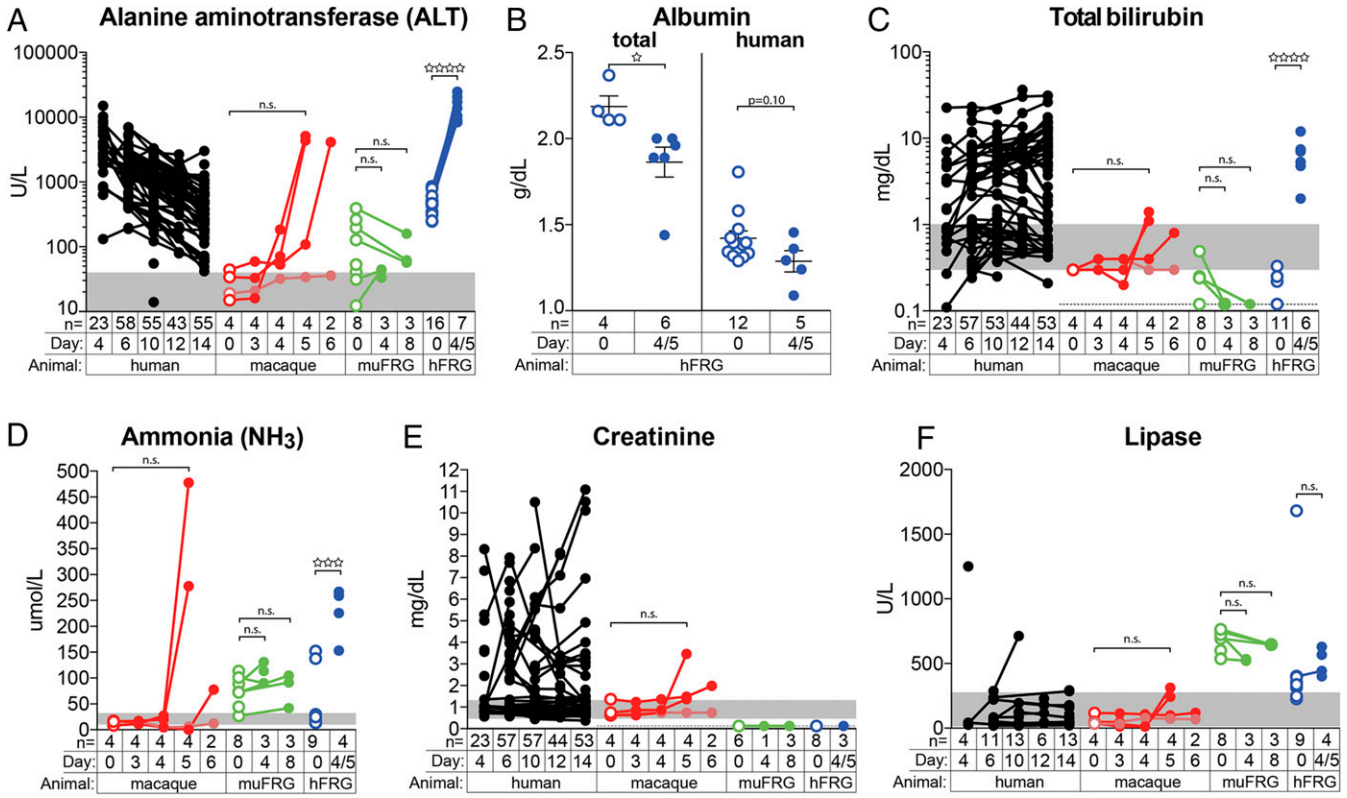

Fig. 4. YFV infection is associated with laboratory abnormalities indicative of severe hepatic injury in humans, macaques, and hFRG mice, but not muFRG mice. Clinical laboratory testing of blood from humans (black), macaques (red), muFRG mice (green), and hFRG mice (blue) was performed to assess end-organ damage for liver [ALT (*A*), albumin (*B*), total bilirubin (*C*), NH_3 (*D*)], kidney (creatinine) (*E*), and pancreas (lipase) (*F*). Human data are shown for comparison; "day" indicates "day post inoculation" for animal models, but for humans "day" indicates "day post hospitalization." Open circles denote preinfection values in animal models and samples from the same individual are connected by a line. Statistical significance was determined from unpaired *t* tests and is denoted by an open star (n.s.: $P \geq 0.05$; ☆: $P = 0.01$ to 0.05; ☆☆☆: $P = 0.0001$ to 0.001; ☆☆☆☆: $P < 0.0001$). Gray areas indicate the human reference range for each parameter, as defined by the American Board of Internal Medicine (67).

human hepatocytes to YFV infection. This enabled the development of a mouse model of YFV infection that recapitulates key aspects of severe YF in humans: greater tropism of YFV in the liver versus the brain; severe hepatitis as defined hepatocyte necrosis; 10- to 40-fold increases in blood ALT concentrations; and coagulopathy as defined by substantial PT prolongation. This model also allowed us to address the relationship between hepatitis and coagulopathy in severe YF. We first clarified the type of coagulopathy present in patients with severe YF. This revealed highly elevated D-dimer concentrations, which demonstrates the presence of a consumptive coagulopathy. A consumptive coagulopathy also was observed in YFV-infected macaques, but not in YFV-infected hFRG mice, despite the ability of blood from hFRG mice to generate human D-dimers ex vivo. The combination of a prolonged PT with no elevation in D-dimer suggests that the coagulopathy observed in YFV-infected hFRG mice is due principally to a decrease in clotting-factor production. It also implies that infection and injury of human hepatocytes alone is insufficient to cause the consumptive coagulopathy observed in severe human cases of YF. Thus, in humans and NHPs, important aspects of YF pathogenesis likely occur in cells and tissues outside of the hepatocellular compartment.

Although consumptive coagulopathy has been hypothesized to contribute to the hemorrhagic manifestations accompanying severe YF, historically there is limited data to support this idea (15, 22). Despite all of the clinical studies of YF in humans over the past 100 y, elevated D-dimers are described in only a few case reports (44, 45). The lack of data regarding the development of coagulopathy in human YF is relevant given the recent trend of treating severe YF with plasma exchange (24). Although data on this intervention is still emerging, preliminary results suggest that coagulopathy may be an important factor in the development of microthrombotic disease, multiorgan failure, and fatal outcome of severe YF cases. As such, the human data presented herein may provide a reference for clinicians to monitor coagulation parameters more closely in YFV-infected patients.

Consumptive coagulopathy is caused by aberrant hyperactivation of the coagulation cascade. Certain drugs (e.g., novoseven) and venom (e.g., Russell's viper) can activate coagulation factors directly, and the ability of YFV proteins to act in a similar fashion cannot be formally excluded. However, coagulopathy in the context of virus infection more often is attributed to induction of a hyperinflammatory state (i.e., "cytokine storm") and concomitant up-regulation of procoagulant molecules, such as tissue factor (46–49). A definitive causal link between acute virus-induced inflammation and the development of coagulopathy in viral hemorrhagic fever has been difficult to define. Infection (and/or activation) of Kupffer and endothelial cells is thought to play a central role in the inflammatory response and consumptive coagulopathy that develops during EBOV infection (23, 49–51), and in vitro studies suggest that both of these cell types could be targets of YFV infection (52–55). Indeed, YFV-17D–infected mice engrafted with human immune cells exhibit higher viral loads and greater disease than mice engrafted with murine immune cells, supporting the idea that direct infection of immune cells also contributes to YF

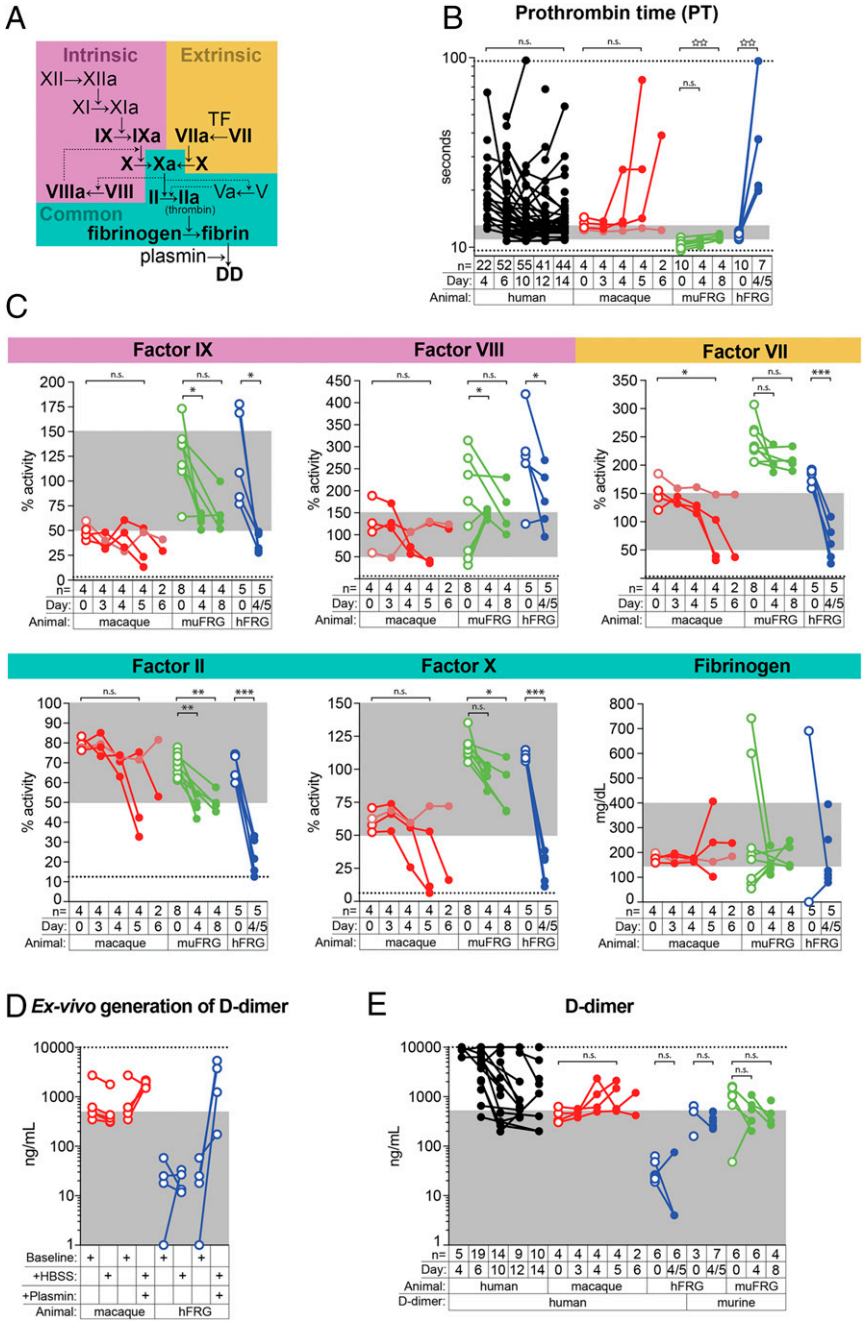

Fig. 5. Coagulation factor consumption is a feature of YFV infection in humans and macaques but not in hFRG mice. (*A*) Simplified scheme of the coagulation cascade. (*B*) PT in humans (black), macaques (red), muFRG mice (green), and hFRG mice (blue). (*B–E*) Solid symbols denote YFV-infected individuals whereas open symbols denote uninfected ones. Dashed lines represent the limits of detection of the assay; gray areas indicate the human reference range for each parameter, as defined by the American Board of Internal Medicine (67). (*C*) Coagulation factor activities determined using factor-deficient human plasma in a PT-based assay. (*D*) Demonstration that plasma from macaques and hFRG mice can generate D-dimers and be detected with the assays used in this study. (*E*) Plasma D-dimer concentrations in YFV-infected humans and animal models. Significance from paired *t* tests is denoted by an asterisk, whereas significance from unpaired *t* tests is denoted by an open star (n.s.: $P \geq 0.05$; ☆☆: $P = 0.001$ to 0.01; *$P = 0.01$ to 0.05; **$P = 0.001$ to 0.01; ***$P = 0.0001$ to 0.001).

pathogenesis (17). Thus, it is conceivable that YFV infection (or activation) of extrahepatic cells could induce consumptive coagulopathy akin to Ebola hemorrhagic fever. Additional research is needed to determine how these extrahepatic cells modulate YF pathogenesis and coagulopathy. Alternatively, the loss of anticoagulant factors (e.g., tissue factor pathway inhibitor, protein C, protein S, antithrombin, and thrombomodulin) via hepatocyte destruction, blood loss, or some other mechanism also could result in an imbalance in the coagulation cascade that promotes the development of consumptive coagulopathy in cases of severe YF.

Our study has limitations, especially regarding comparisons of YF pathogenesis among host species (i.e., human, macaque, and mouse). First, the South American strain of YFV infecting humans in Brazil is ∼90% identical at the amino acid level to the West African strain used in our animal models, and it is possible

that this sequence variation could explain some of the discrepancies observed between humans and animals in this study. Second, the dose and route of infection were different for each animal species: naturally infected humans likely were inoculated by mosquito bite with an unknown dose in the range of 10^4 to 10^6 infectious units (56); macaques were inoculated s.c. with 5.5×10^2 FFU (5×10^4 $TCID_{50}$); and mice were inoculated i.v. with 2×10^5 FFU. However, the detection of YFV RNA in the blood of infected humans, macaques, and mice implies that YFV circulates in each of these hosts. Our study also was limited by each host in species-specific ways. In humans, the time between YFV inoculation and the onset of symptoms is variable (57), which precludes a detailed analysis of the early events in pathogenesis. The macaque model allowed for a more controlled examination of YF over time, but the small sample size ($n = 4$) and lack of overt disease in one animal results in an underpowered study for detailed statistical analysis. The hFRG mouse model afforded a larger sample size but fewer time points due to rapid death. Importantly, FRG mice lack functional lymphocytes, which could be a target of YFV infection and undoubtedly contribute to the immune response to YFV infection in immunocompetent humans and nonhuman primates. As a result, the role of the immune response in the development of coagulopathy—especially in the context of hepatocyte infection by YFV—remains unexplored. Patchy engraftment of human hepatocytes also results in a relatively disorganized liver architecture, which could modulate YFV pathogenesis through gene expression alterations that are unique to the hFRG model (58). The hepatocellular chimerism in hFRG mice also creates a chimeric human–mouse coagulation cascade. Inefficient interactions between specific human and murine coagulation factors have been described and could impact clotting depending on the percentage of chimerism in a given individual (59, 60). For this reason, we limited our coagulation analyses to functional clotting-based assays or tests that quantify the concentration of an analyte (e.g., D-dimer) in blood from each animal studied. While we cannot definitively exclude the possibility that the murine coagulation system contains inhibitors that prevent the development of consumptive coagulopathy in hFRG mice, our ability to generate D-dimers in plasma from this host ex vivo makes this less likely. Despite the limitations associated with the study of YF in each host by itself, our data provide added insight into pathogenesis and coagulopathy, which has implications for therapeutic interventions against YF and possibly other emerging RNA viruses (e.g., SARS-CoV-2 and Ebolavirus) that also cause coagulation defects.

Methods

Human Subjects. The human data used in this study were collected as part of an ongoing institutional review board-approved study at the Clinical Hospital of the University of São Paulo School of Medicine and the Infectious Diseases Institute Emilio Ribas, São Paulo, Brazil (CAAE: 59542216.3.1001.0068). All study participants or their legal representatives provided signed informed consent to participate in this study. Protected health information was maintained in secured cabinets and electronic files using the REDCap platform on a secured server at the School of Medicine, University of São Paulo.

Mice. All mouse experiments were conducted under a Washington University School of Medicine Institutional Animal Care and Use Committee approved protocol in compliance with the Animal Welfare Act. WT C57BL/6J mice (male and female) were purchased from The Jackson Laboratory. hFRG mice were generated by Yecuris Corporation and maintained according to their specific care and use guidelines. In brief, FRG triple knockout mice (*Fah*$^{-/-}$, *Rag2*$^{-/-}$, and *Il2rγ*$^{-/-}$ on a C57BL/6J background) were fed a diet supplemented orally with nistinone (CurX Nistinone, Yecuris) in the drinking water. At 6 wk of age, nistinone was removed from drinking water and a urokinase-type plasminogen-activator–expressing adenoviral vector was delivered via i.v. injection to induce hepatocellular death, which was accompanied by intrasplenic injection of $\sim 5 \times 10^5$ cryopreserved human hepatocytes. Engraftment of human hepatocytes was monitored by assessing blood concentrations of human albumin. Only mice with human albumin levels of ≥5.0 mg/mL of plasma (corresponding to ≥70% engraftment) were used for this study. Engraftment of FAH$^{+/+}$ murine hepatocytes into the FRG mice were generated using similar methods. Adult mice of both sexes, ages 12 to –24 wk, were used for this study. FRG mice continued on their regular diet of PicoLab High Energy Mouse Diet, 5LJ5 chow (LabDiet), and 3.25% wt/vol dextrose-water during infection experiments.

Macaques. Rhesus macaques were managed in accordance with the recommendations described in the Guide for the Care and Use of Laboratory Animals of the National Institute of Health (61), the Office of Animal Welfare, and the US Department of Agriculture. All animal work was approved by the Oregon National Primate Research Center (ONPRC) Institutional Animal Care and Use Committee (Public Health Service Office of Laboratory Animal Welfare Assurance #A3304-01). The ONPRC is fully accredited by the Assessment and Accreditation of Laboratory Animal Care International. All procedures were carried out under anesthesia induced by ketamine by trained personnel under the supervision of veterinary staff. After infection, trained personnel monitored animals four times each day. Animals were euthanized humanely by veterinary staff in accordance with end-point policies. Euthanasia was conducted under anesthesia with ketamine followed by overdose with sodium pentobarbital. This method is consistent with the recommendation of the American Veterinary Medical Association.

Biosafety. All aspects of this study were approved by the offices of Environmental Health and Safety at Washington University School of Medicine and ONPRC prior to the initiation of this study. All personnel working in rooms in which pathogenic YFV was used were vaccinated at least 2 wk prior to initiating work. Studies involving animals were performed in an A-BSL-3 suite by personnel equipped with powered air purifying respirators. Non-animal studies involving infectious virus were performed in a BSL-3 laboratory with appropriate barrier personal protective equipment.

Viruses. The YFV-DakH1279 strain (YFV-Dakar) was isolated from a human in Senegal in 1965 and obtained from the World Reference Center for Emerging Viruses and Arboviruses (K. Plante, R, Tesh, and S. Weaver, University of Texas Medical Branch). The viral stock used to infect mice was grown on Vero-WHO cells that were maintained in Dulbecco's Modified Eagle Media with 5% fetal bovine serum. Supernatant was harvested upon observation of cytopathic effect. Debris was removed by centrifugation, and stocks were aliquoted and stored at –80 °C. The stock used to infect rhesus macaques was passaged through a single macaque and then propagated in C6/36 cells. Mice were inoculated with 2×10^5 FFU of YFV via inoculation of 50 μL into the retroorbital venous plexus. Macaques were inoculated via a s.c. route (1.0 mL divided among five injection sites) with a total of 5.5×10^2 FFU (i.e., 5×10^4 $TCID_{50}$) (62).

Focus-Forming Assay. Vero-WHO cells were seeded at a density of 2.5×10^4 cells per well in flat-bottom 96-well tissue culture plates. The following day, medium was removed and replaced with 100 μL of 10-fold serial dilutions of virus containing solutions. Two hours later, 135 μL of methylcellulose overlay was added. Plates were incubated for 48 h and then fixed with 4% paraformaldehyde in phosphate-buffered saline for 10 min, followed by permeabilization with saponin-containing buffer. Plates were incubated overnight at 4 °C in 100 μL of permeabilization buffer containing a mixture of 4G2 and E60 (63–65) monoclonal antibodies, each at 0.5 μg/mL. Goat anti-mouse secondary antibody (Sigma) was used at a concentration of 1:2,000, and foci were scanned and quantitated on a Biospot plate reader (Cellular Technology).

Quantitative RT-PCR. We developed a primer/probe set for real-time PCR of YFV based upon the assay developed in ref. 66 that targets the 5′ untranslated region: F—5′-AGGTGCATTGGTCTGCAAAT-3′; R—5′-TCTCTGCTAATCGCTCAAIG-3′; P—5′-/56-FAM/GTTGCTAGGCAATAAACACATTTGGA/3BHQ_1/-3′. An RNA standard was made by amplifying a 590-bp product containing the real-time PCR primer-binding sites from the YFV-Dakar genome (F—5′-AGGTGCATTGGT CTGCAAAT-3′; R—5′-AATCTGGGCACCAGAACTTG-3′) and cloning this into Zero Blunt PCR vector (Invitrogen). After linearization of the construct (HindIII, New England BioLabs), transcription was performed in vitro for 6 h (MEGAscript T7 transcription kit, Invitrogen) followed by purification (MEGAclear transcription cleanup kit, Invitrogen), quantification, and dilution to a concentration of 1×10^{10} transcript copies/microliter. Ten-fold dilutions of this transcript were used as a standard curve, which was linear over eight orders of magnitude and sensitive down to 10 copies of RNA transcript per reaction.

Viral RNA was extracted on the KingFisher Flex System (ThermoFisher) according to the manufacturer's instructions using the MagMAX Viral RNA or mirVana Total RNA kits for plasma and tissues, respectively. RNA was reverse-transcribed and amplified using the TaqMan RNA-to-CT 1-Step Kit (ThermoFisher) on the QuantStudio 6 Flex Real-Time PCR System. Reverse transcription was carried out at 48 °C for 15 min followed by 2 min at 95 °C. Amplification was accomplished over 50 cycles as follows: 95 °C for 15 s and 60 °C for 1 min. The reaction mixture contained final concentrations of primers and probes of 500 and 100 nM, respectively.

Tissue Collection. Mice were sedated with i.p. administration of ketamine. Blood was drawn from the right ventricle. The entire cardiovascular tree was perfused with ∼20 mL of saline administered via canulation of the left ventricle. Midway through perfusion, the superior vena cava was transected to allow for outflow of fluid from the vasculature. The left liver lobe was added to 10 mL of 10% neutral buffered formalin. The remaining lobes were snap-frozen in tubes. The brain was transected in the sagittal plane: one hemisphere was placed in 10% neutral buffered formalin and the other half was snap-frozen. A similar euthanasia and perfusion scheme was performed on macaques.

Coagulation Factor Assays. For mice, PT was measured from whole blood, obtained either by phlebotomy of a facial vein (for survival procedures) or cardiac puncture (for terminal procedures) using the point-of-care CoaguChek instrument (Roche). For macaques, PT was performed on the Coatron X Pro (Teco) using citrated plasma according to the manufacturer's instructions. For both mice and macaques, levels of factors II, VII, VIII, IX, and X were measured on the Coatron X pro using a PT-based assay according to the manufacturer's recommendations. All coagulation assays were performed in a biosafety cabinet under BSL-3 conditions.

D-Dimer Measurement. Plasma D-dimer concentrations were analyzed in YF patients by the clinical laboratory at the University of Sao Paulo using HemosIL D-dimer HS 500, an automated, latex-enhanced turbidimetric immunoassay for the quantitative determination of D-dimer, according to the manufacturer's instructions. The upper limit of the analytical measurement range for this assay is 10,000 ng/mL. Some of the clinical samples that registered at this level were diluted and retested. For consistency, all values >10,000 ng/mL have been reported as 10,000 ng/mL. Human D-dimer testing on citrated plasma from hFRG mice was performed on the Coatron X pro using the Blue D-dimer latex agglutination assay (Teco) according to the manufacturer's instructions. D-dimer testing on citrated plasma from macaques was performed on the Coatron X pro using Stago's D-Di Liatest (Stago Diagnostica); control samples were used to calibrate the Stago assay for use on the Coatron X pro. Murine D-dimer concentrations were assayed using the Mouse D2D(D-Dimer) ELISA Kit (Elabscience). The in vitro D-dimer generation assay was performed as follows: 10 μL of human plasmin (Millipore-Sigma), reconstituted to 1 unit/mL in Hank's Balanced Salt Solution (HBSS), was added to 30 μL of citrated plasma, vortexed, and incubated at 37 °C for 10 min. A total of 10 μL of PT reagent was added, vortexed, and incubated at 37 °C for 20 min. Then 25 μL of this mixture was tested for the formation of D-dimer using the Coatron X pro latex agglutination D-dimer assay. This assay was used to determine the validity of each assay for each species. No latex-agglutination assay for mouse D-dimer was identified, and so D-dimer analysis was not performed on muFRG or WT mice.

Clinical Chemistries. Prior to analysis, citrated plasma was mixed 1:9 with 10% Triton X-100 in HBSS (1% final volume of Triton-X-100) and then incubated at room temperature for 1 h to inactivate infectious virus. This method of virus inactivation was found to not affect the clinical chemistry analyses. Specimens were analyzed using the Catalyst One Chemistry Analyzer (IDEXX Laboratories). Some specimens required dilutions to achieve an ALT value within the analytical measurement range; in these instances, dilution was performed in HBSS (or deionized H_2O for macaque samples), and the value was corrected by the final dilution factor. Human-specific albumin was measured using the Human Albumin ELISA Kit (Bethyl Laboratories).

Histological Assessment. Hematoxylin- and eosin-stained formalin-fixed paraffin-embedded (FFPE) histologic sections of mouse and nonhuman primate livers were reviewed by two board-certified fellowship-trained hepatopathologists (L.I.K. and K.B.) for percentage of engraftment (hFRG group only) and percentage of necrosis (all groups) in consultation with a Brazilian pathologist (A.N.D.-N.) experienced in examining YFV-infected livers. The pathologists were blinded to YFV infection status within individual groups. Whole slide images were obtained using an Aperio CS scanner (Leica) and viewed using the image analysis software HALO (Indica Labs, v2.2.1870.8). Individual microscopic images were taken using an Olympus BX51/3 or Nikon Eclipse E3400 microscope with attached camera at the magnifications as indicated in each figure legend.

In Situ Hybridization and Immunohistochemistry. Viral RNA was visualized by in situ hybridization using a custom YFV-Dakar probe and the RNAscope 2.0 HD detection kit (Advanced Cell Diagnostics) according to the manufacturer's instructions. Immunohistochemical (IHC) staining of FFPE sections for FAH was performed using a polyclonal rabbit antibody (Invitrogen catalog #PA5-42050) after standard deparaffinization, rehydration, peroxidase blocking, and antigen retrieval with boiling citrate solution (pH of 6) for 30 min.

Statistical Analysis. Statistical analyses were performed in Prism 7 (Graphpad Software). Each statistical test used is denoted in the figure legends.

Data Availability. All study data are included in the article and supporting information.

ACKNOWLEDGMENTS. We thank the patients and their families or legal representatives for providing consent and assisting with the present study; the health professional staff from the Institute of Infectious Diseases Emilio Ribas and the Hospital das Clínicas, School of Medicine, University of São Paulo, for their support; the animal care technicians and veterinarians at Washington University School of Medicine and Oregon Health Sciences University and the pathology assistants, residents, and staff of the Pathology Department of the Faculty of Medicine of the University of São Paulo who participated in the autopsies of YF victims; Drs. George Broze, Jorge DiPaola, and Thomas Girard for insightful coagulation advice; Dr. Daniel Streblow for contributing naive macaque tissue for histological comparison; and Dr. Thomas Monath for providing constructive criticism of the manuscript. This study was funded, in part, by National Institutes of Health (NIH) Grant R01 AI073755 (to M.S.D). YFV infection of macaques was funded by NIH Grant R44 AI079898 (to M.K.S) and Oregon National Primate Research Center NIH Grant P51 OD011092 (to M.K.S.). L.-I.K was supported by NIH Grant T32 EB021955. The YF-autopsy project was partially funded by the Fundação de Amparo à Pesquisa do Estado de São Paulo (FAPESP) (process no. 2013/21728-2). The patient cohort was partially funded by São Paulo Research Foundation (FAPESP Grant 2016/01735-2).

1. D. M. Knipe, P. M. Howley, Eds., *Fields Virology* (Wolters Kluwer/Lippincott Williams & Wilkins Health, ed. 6, 2013).
2. F. Douam, A. Ploss, Yellow fever virus: Knowledge gaps impeding the fight against an old foe. *Trends Microbiol.* **26**, 913–928 (2018).
3. R. Klitting, E. A. Gould, C. Paupy, X. de Lamballerie, What does the future hold for yellow fever virus? (I). *Genes (Basel)* **9**, 291 (2018).
4. T. P. Monath, P. F. C. Vasconcelos, Yellow fever. *J. Clin. Virol.* **64**, 160–173 (2015).
5. World Health Organization, Situation report. Yellow fever. (2016). https://www.who.int/emergencies/yellow-fever/situation-reports/28-october-2016/en/. Accessed 16 November 2020.
6. World Health Organization, Emergencies preparedness, response: Brazil—Yellow fever. (2019). https://www.who.int/csr/don/11-february-2019-yellow-fever-brazil/en/. Accessed 16 November 2020.
7. M. D. P. Cunha *et al*., Origin of the São Paulo Yellow Fever epidemic of 2017–2018 revealed through molecular epidemiological analysis of fatal cases. *Sci. Rep.* **9**, 20418 (2019).
8. F. V. Ajogbasile *et al*., Real-time metagenomic analysis of undiagnosed fever cases unveils a yellow fever outbreak in Edo State, Nigeria. *Sci. Rep.* **10**, 3180 (2020).
9. World Health Organization, Yellow fever, chap. 2, WHO report on global surveillance of epidemic-prone infectious diseases (2000). https://www.who.int/csr/resources/publications/surveillance/Yellow_fever.pdf?ua=1. Accessed 16 November 2020.
10. B. R. Ellis, A. D. T. Barrett, The enigma of yellow fever in East Africa. *Rev. Med. Virol.* **18**, 331–346 (2008).
11. F. M. Shearer *et al*., Global yellow fever vaccination coverage from 1970 to 2016: An adjusted retrospective analysis. *Lancet Infect. Dis.* **17**, 1209–1217 (2017).
12. M. Theiler, H. H. Smith, The use of yellow fever virus modified by in vitro cultivation for human immunization. *J. Exp. Med.* **65**, 787–800 (1937).
13. F. M. Shearer *et al*., Existing and potential infection risk zones of yellow fever worldwide: A modelling analysis. *Lancet Glob. Health* **6**, e270–e278 (2018).
14. D. Musso, P. Parola, D. Raoult, Yellow fever: The Pacific should be prepared. *Lancet* **392**, 2347 (2018).
15. T. P. Monath, A. D. Barrett, Pathogenesis and pathophysiology of yellow fever. *Adv. Virus Res.* **60**, 343–395 (2003).
16. N. W. Elton, A. Romero, A. Trejos, Clinical pathology of yellow fever. *Am. J. Clin. Pathol.* **25**, 135–146 (1955).

17. F. Douam *et al.*, Single-cell tracking of flavivirus RNA uncovers species-specific interactions with the immune system dictating disease outcome. *Nat. Commun.* **8**, 14781 (2017).
18. S. E. Woodson, A. N. Freiberg, M. R. Holbrook, Differential cytokine responses from primary human Kupffer cells following infection with wild-type or vaccine strain yellow fever virus. *Virology* **412**, 188–195 (2011).
19. K. C. Meier, C. L. Gardner, M. V. Khoretonenko, W. B. Klimstra, K. D. Ryman, A mouse model for studying viscerotropic disease caused by yellow fever virus infection. *PLoS Pathog.* **5**, e1000614 (2009).
20. T. P. Monath, K. R. Brinker, F. W. Chandler, G. E. Kemp, C. B. Cropp, Pathophysiologic correlations in a rhesus monkey model of yellow fever with special observations on the acute necrosis of B cell areas of lymphoid tissues. *Am. J. Trop. Med. Hyg.* **30**, 431–443 (1981).
21. F. Liprandi, R. Walder, Replication of virulent and attenuated strains of yellow fever virus in human monocytes and macrophage-like cells (U937). *Arch. Virol.* **76**, 51–61 (1983).
22. L. H. Dennis, B. E. Reisberg, J. Crosbie, D. Crozier, M. E. Conrad, The original haemorrhagic fever: Yellow fever. *Br. J. Haematol.* **17**, 455–462 (1969).
23. A. K. McElroy *et al.*, Ebola hemorrhagic fever: Novel biomarker correlates of clinical outcome. *J. Infect. Dis.* **210**, 558–566 (2014).
24. E. G. Kallas, A. Wilder-Smith, Managing severe yellow fever in the intensive care: Lessons learnt from Brazil. *J. Travel Med.* **26**, taz043 (2019).
25. C. R. L. Webster, Hemostatic disorders associated with hepatobiliary disease. *Vet. Clin. North Am. Small Anim. Pract.* **47**, 601–615 (2017).
26. L. Miorin *et al.*, Host-specific NS5 ubiquitination determines yellow fever virus tropism. *J. Virol.* **93**, e00151-19 (2019).
27. L. K. M. Lam, A. M. Watson, K. D. Ryman, W. B. Klimstra, Gamma-interferon exerts a critical early restriction on replication and dissemination of yellow fever virus vaccine strain 17D-204. *NPJ Vaccines* **3**, 5 (2018).
28. A. K. Erickson, J. K. Pfeiffer, Spectrum of disease outcomes in mice infected with YFV-17D. *J. Gen. Virol.* **96**, 1328–1339 (2015).
29. L. O. Berthelsen, A. T. Kristensen, M. Tranholm, Animal models of DIC and their relevance to human DIC: A systematic review. *Thromb. Res.* **128**, 103–116 (2011).
30. M. Theiler, Studies on the action of yellow fever virus in mice. *Ann. Trop. Med. Parasitol.* **24**, 249–272 (1930).
31. H. Azuma *et al.*, Robust expansion of human hepatocytes in Fah-/-/Rag2-/-/Il2rg-/- mice. *Nat. Biotechnol.* **25**, 903–910 (2007).
32. E. G. Kallas *et al.*, Predictors of mortality in patients with yellow fever: An observational cohort study. *Lancet Infect. Dis.* **19**, 750–758 (2019).
33. F. Engelmann *et al.*, Pathophysiologic and transcriptomic analyses of viscerotropic yellow fever in a rhesus macaque model. *PLoS Negl. Trop. Dis.* **8**, e3295 (2014).
34. R. A. Mason, N. M. Tauraso, R. O. Spertzel, R. K. Ginn, Yellow fever vaccine: Direct challenge of monkeys given graded doses of 17D vaccine. *Appl. Microbiol.* **25**, 539–544 (1973).
35. A. D. Barrett, E. A. Gould, Comparison of neurovirulence of different strains of yellow fever virus in mice. *J. Gen. Virol.* **67**, 631–637 (1986).
36. T. J. Chambers, M. Nickells, Neuroadapted yellow fever virus 17D: Genetic and biological characterization of a highly mouse-neurovirulent virus and its infectious molecular clone. *J. Virol.* **75**, 10912–10922 (2001).
37. J. J. Schlesinger *et al.*, Replication of yellow fever virus in the mouse central nervous system: Comparison of neuroadapted and non-neuroadapted virus and partial sequence analysis of the neuroadapted strain. *J. Gen. Virol.* **77**, 1277–1285 (1996).
38. P. Meuleman *et al.*, Morphological and biochemical characterization of a human liver in a uPA-SCID mouse chimera. *Hepatology* **41**, 847–856 (2005).
39. Y.-L. Ho *et al.*; Hospital das Clínicas Yellow Fever Assistance Group, Severe yellow fever in Brazil: Clinical characteristics and management. *J. Travel Med.* **26**, taz040 (2019).
40. M. Theiler, Susceptibility of white mice to the virus of yellow fever. *Science* **71**, 367 (1930).
41. W. A. Sawyer, W. Lloyd, The use of mice in tests of immunity against yellow fever. *J. Exp. Med.* **54**, 533–555 (1931).
42. R. B. Tesh *et al.*, Experimental yellow fever virus infection in the Golden Hamster (Mesocricetus auratus). I. Virologic, biochemical, and immunologic studies. *J. Infect. Dis.* **183**, 1431–1436 (2001).
43. E. Sbrana, S.-Y. Xiao, V. L. Popov, P. C. Newman, R. B. Tesh, Experimental yellow fever virus infection in the golden hamster (Mesocricetus auratus) III. Clinical laboratory values. *Am. J. Trop. Med. Hyg.* **74**, 1084–1089 (2006).
44. Z. Chen *et al.*, A fatal yellow fever virus infection in China: Description and lessons. *Emerg. Microbes Infect.* **5**, e69 (2016).
45. M. C. de Paiva, A. Prata, R. C. S. Moura, A. V. Pinto, F. Santos, Estudo da coagulação em um caso de hepatite de lábrea [in Portuguese]. *Rev. Soc. Bras. Med. Trop.* **17**, 37–40 (1984).
46. I. Messaoudi, C. F. Basler, Immunological features underlying viral hemorrhagic fevers. *Curr. Opin. Immunol.* **36**, 38–46 (2015).
47. B. D. Moore *et al.*, Virulent and avirulent strains of equine arteritis virus induce different quantities of TNF-alpha and other proinflammatory cytokines in alveolar and blood-derived equine macrophages. *Virology* **314**, 662–670 (2003).
48. S. Baize *et al.*, Inflammatory responses in Ebola virus-infected patients. *Clin. Exp. Immunol.* **128**, 163–168 (2002).
49. T. W. Geisbert *et al.*, Mechanisms underlying coagulation abnormalities in ebola hemorrhagic fever: Overexpression of tissue factor in primate monocytes/macrophages is a key event. *J. Infect. Dis.* **188**, 1618–1629 (2003).
50. H. Feldmann *et al.*, Filovirus-induced endothelial leakage triggered by infected monocytes/macrophages. *J. Virol.* **70**, 2208–2214 (1996).
51. E. I. Ryabchikova, L. V. Kolesnikova, S. V. Luchko, An analysis of features of pathogenesis in two animal models of Ebola virus infection. *J. Infect. Dis.* **179** (suppl. 1), S199–S202 (1999).
52. S. F. Khaiboullina, A. A. Rizvanov, M. R. Holbrook, S. St Jeor, Yellow fever virus strains Asibi and 17D-204 infect human umbilical cord endothelial cells and induce novel changes in gene expression. *Virology* **342**, 167–176 (2005).
53. S. E. Woodson, M. R. Holbrook, Infection of hepatocytes with 17-D vaccine-strain yellow fever virus induces a strong pro-inflammatory host response. *J. Gen. Virol.* **92**, 2262–2271 (2011).
54. S. E. Woodson, A. N. Freiberg, M. R. Holbrook, Coagulation factors, fibrinogen and plasminogen activator inhibitor-1, are differentially regulated by yellow fever virus infection of hepatocytes. *Virus Res.* **175**, 155–159 (2013).
55. B. Szotowski, S. Antoniak, W. Poller, H.-P. Schultheiss, U. Rauch, Procoagulant soluble tissue factor is released from endothelial cells in response to inflammatory cytokines. *Circ. Res.* **96**, 1233–1239 (2005).
56. L. M. Styer *et al.*, Mosquitoes inoculate high doses of West Nile virus as they probe and feed on live hosts. *PLoS Pathog.* **3**, 1262–1270 (2007).
57. M. A. Johansson, N. Arana-Vizcarrondo, B. J. Biggerstaff, J. E. Staples, Incubation periods of Yellow fever virus. *Am. J. Trop. Med. Hyg.* **83**, 183–188 (2010).
58. N. Aizarani *et al.*, A human liver cell atlas reveals heterogeneity and epithelial progenitors. *Nature* **572**, 199–204 (2019).
59. J. J. Emeis *et al.*, A guide to murine coagulation factor structure, function, assays, and genetic alterations. *J. Thromb. Haemost.* **5**, 670–679 (2007).
60. T. Knudsen, O. H. Olsen, L. C. Petersen, Tissue factor and factor VIIa cross-species compatibility. *Front. Biosci.* **16**, 3196–3215 (2011).
61. National Research Council, *Guide for the Care and Use of Laboratory Animals* (National Academies Press, Washington, DC, ed. 8, 2011).
62. E. Hammarlund *et al.*, A flow cytometry-based assay for quantifying non-plaque forming strains of yellow fever virus. *PLoS One* **7**, e41707 (2012).
63. M. K. Gentry, E. A. Henchal, J. M. McCown, W. E. Brandt, J. M. Dalrymple, Identification of distinct antigenic determinants on dengue-2 virus using monoclonal antibodies. *Am. J. Trop. Med. Hyg.* **31**, 548–555 (1982).
64. E. A. Henchal, M. K. Gentry, J. M. McCown, W. E. Brandt, Dengue virus-specific and flavivirus group determinants identified with monoclonal antibodies by indirect immunofluorescence. *Am. J. Trop. Med. Hyg.* **31**, 830–836 (1982).
65. T. Oliphant *et al.*, Antibody recognition and neutralization determinants on domains I and II of West Nile Virus envelope protein. *J. Virol.* **80**, 12149–12159 (2006).
66. A. Rojas *et al.*, Internally controlled, multiplex real-time reverse transcription PCR for dengue virus and yellow fever virus detection. *Am. J. Trop. Med. Hyg.* **98**, 1833–1836 (2018).
67. American Board of Internal Medicine, ABIM laboratory test reference ranges—January 2020.